International Journal of Pharmaceutics 421 (2011) 12–23

Contents lists available at SciVerse ScienceDirect

International Journal of Pharmaceutics

journal homepage: www.elsevier.com/locate/ijpharm

Effect of carrier particle shape on dry powder inhaler performance

Waseem Kaialy[a,b,c], Amjad Alhalaweh[b], Sitaram P. Velaga[b], Ali Nokhodchi[a,*]

[a] Chemistry and Drug Delivery Group, Medway School of Pharmacy, University of Kent, ME4 4TB, Kent, UK
[b] Pharmaceutical Engineering group, Department of Health Sciences, Luleå University of Technology, Lulea S-971 87, Sweden
[c] Pharmaceutics and Pharmaceutical Technology Department, University of Damascus, Syria

ARTICLE INFO

Article history:
Received 27 July 2011
Received in revised form 8 September 2011
Accepted 13 September 2011
Available online 17 September 2011

Keywords:
Mannitol
Lactose
Carrier shape
Flow properties
Crystal form
Salbutamol sulphate
Uniformity
Aerosolisation performance

ABSTRACT

The aim of this study was to characterise the aerosolisation properties of salbutamol sulphate (SS) from dry powder inhaler (DPI) formulations containing different carrier products. The difference in the elongation ratio (ER) of the different carriers was highlighted. Different set of carriers, namely commercial mannitol (CM), commercial lactose (CL), cooling crystallised mannitol (CCM), acetone crystallised mannitol (ACM) and ethanol crystallised mannitol (ECM) were used and inspected in terms of size, shape, density, crystal form, flowability, and *in vitro* aerosolisation performance using Multi Stage Liquid Impinger (MSLI) and Aerolizer® inhaler device. Solid-state and morphological characterization showed that CM product was in pure β-form having particles with smaller ER (CM: ER = 1.62 ± 0.04) whereas ACM and ECM mannitol particles were in pure α form with higher ER (ACM: ER = 4.83 ± 0.18, ECM: ER = 5.89 ± 0.19). CCM product crystallised as mixtures of β-form and δ-form and showed the largest variability in terms of particle shape, size, and DPI performance. Linear relationships were established showing that carrier products with higher ER have smaller bulk density (D_b), smaller tap density (D_t), higher porosity (P), and poorer flow properties. *In vitro* aerosolisation assessments showed that the higher the ER of the carrier particles the greater the amounts of SS delivered to lower airway regions indicating enhanced DPI performance. Yet, DPI performance enhancement by increasing carrier ER reached a "limit" as increasing carrier ER from 4.83 ± 0.18 (ACM) to 5.89 ± 0.19 (ECM) did not significantly alter fine particle fraction (FPF) of SS. Also, carrier particles with higher ER were disadvantageous in terms of higher amounts of SS remained in inhaler device (drug loss) and deposited on throat. Linear relationship was established (r^2 = 0.87) showing that the higher the carrier ER the lower the drug emission (EM) upon inhalation. Moreover, poorer flowability for carrier products with higher ER is disadvantageous in terms of DPI formulation dose metering and processing on handling scale. In conclusion, despite that using carrier particles with higher ER can considerably increase the amounts of drug delivered to lower airway regions; this enhancement is restricted to certain point. Also, other limitations should be taken into account including higher drug loss and poorer flowability.

1. Introduction

Efficient drug delivery to the lungs through dry powder inhalers (DPIs) is dependent on several factors including inhaler device, formulation, and inhalation manoeuvre. Preparing ideal DPI formulations requires control overall formulation characteristics at particulate and bulk level to ensure the drug delivery to lower airway regions (Malcolmson and Embleton, 1998; Heyder et al., 1986). In DPI formulations, it is customary to blend micronized drug particles (less than 5 μn in size) with larger carrier particles to address flowability and dose variability issues (Telko and Hickey, 2005; Feeley et al., 1998). The typical concentration of drug in drug–carrier DPI formulations is low (e.g. 1 drug: 67.5 carrier) (Timsina et al., 1994) as in the case of Ventolin Rotocaps® (Glaxo) and cyclohaler® (Pharbita). Therefore, during drug–carrier mixing, drug particles will preferably adhere to the active binding sites (more adhesive areas (Hersey, 1975)) on the carrier surface and expected to separate from carrier surface upon inhalation. Drug re-dispersion is considered most important for getting drug particles into deep lung airway regions (Zeng et al., 2000). Usually, only small amounts of drug reaches the lower airway regions due to strong drug–carrier adhesion (Young et al., 2005). Indeed, drug re-dispersion is a function of balance between cohesive forces (between the drug particles) and the adhesive forces (between drug and carrier particles) (Frijlink and De Boer, 2004). In order to aerosolise drug particles, patient inspiratory force should overcome drug–carrier adhesive forces which are dependent on physicochemical properties of both drug

* Corresponding author. Tel.: +44 1634 202947; fax: +44 1634 883927.
E-mail address: a.nokhodchi@kent.ac.uk (A. Nokhodchi).

0378-5173/$ – see front matter © 2011 Elsevier B.V. All rights reserved.
doi:10.1016/j.ijpharm.2011.09.010

particles and carrier particles (Prime et al., 1997; Berard et al., 2002; Ferron, 1994). Consequently, the characteristics of carrier particles must be well-controlled in terms of size, morphology, crystal form, surface energy, etc. It has been reported that the differences in carrier particle size is likely to have significant impact on DPI aerosolisation performance (Steckel and Müller, 1997). The presence of fine particles on carrier surface may decrease the drug–carrier contact area and consequently drug–carrier adhesion forces leading to improved DPI performance (Louey et al., 2003). Better aerosolisation performance was observed when the carrier tap density was higher (Kaialy et al., 2011a), whereas no correlation was found between carrier flowability and DPI performance (Kaialy et al., 2011b; Louey and Stewart, 2002). Carriers with reduced dispersive surface energy produced higher fine particle fraction (FPF) of the drug upon aerosolisation (Sethuraman and Hickey, 2002). Carrier particles with higher elongation ratio (Hamishehkar et al., 2010) or increased surface roughness (Kaialy et al., in press) showed favorable inhalation properties.

In this paper, in order to improve the understanding of the effect of carrier physical properties on DPI performance, the influence of using carrier particles with considerably different morphologies on the content uniformity and inhalation behaviour of a model drug (salbutamol sulphate) from Aerolizer® DPI inhaler device were investigated.

2. Materials and methods

2.1. Materials

Micronized Salbutamol Sulphate (LB Bohle, Germany) was employed as a model drug ($d_{50\%}$ = 1.8 ± 0.3 μm). Mannitol, acetone, and absolute ethanol were supplied from Fisher Scientific, UK. Lactose was obtained from DMV International, Netherlands.

2.2. Preparing of different carrier products

Five different carrier powders were investigated including commercial mannitol (CM), commercial lactose (CL), cooling crystallised mannitol (CCM), acetone crystallised mannitol (ACM) and ethanol crystallised mannitol (ECM). CM and CL and were used as received from suppliers. CCM product was prepared as follows: 5 g of mannitol was dissolved in 25 mL deionised water to prepare 20% saturated solution of mannitol under heating (40 °C) and stirring (250 rpm). Once prepared, mannitol saturated solution was removed from heating and left uncovered in ambient conditions (22 °C, 50% RH) for 96 h. After that, CCM particles were collected by spatula and transferred to watch glass for further drying. The watch glass containing CCM particles were left to dry in drying oven for 24 h at 80 °C after which they were transferred to glass vials and sealed until required. The yield was 97.60% for this sample. ACM (Kaialy et al., 2010a) and ECM (Kaialy et al., 2010b) were prepared using the published methods. DSC traces showed that no water was associated with mannitol crystallised samples after drying (figures not shown).

The reproducibility of the crystallization technique for crystallised mannitol powder was tested by making 3 batches. Analysis on each specific batch demonstrated that, when stored at ambient conditions (22 °C, 50% RH); solid state, size, and aerosolisation performance was not significantly influenced.

2.3. Sieving

In order to limit the effect of carrier particle size, all carrier powders were sieved to separate particles in geometric size fractions of 63–90 μm (Bell et al., 2006; Byron and Jashnam, 1990; Steckel et al., 2004). These size fractions were obtained after mechanical sieving by pouring each carrier powder onto the top of 90 μm sieve which was placed above 63 μm sieve. The sieve shaker (Retsch® Gmbh Test Sieve, Germany) was then operated for 15 min. After the sieving process was complete, the particles retained on the 63 μm sieve were collected and stored in sealed glass vials until required for further investigation. All investigations described below on carriers were performed on the 63–90 μm size fractions.

2.4. Image analysis using optical microscopy

Dynamic shape analysis was employed to assess particle shape of different carriers using image analysis software (designed in-house at King's College, London) installed on an Archimedes computer attached to an optical microscope (Nikon Labophot, Tokyo, Japan) via a miniature video camera). For each carrier sample, a micro-spatula was used to sample about 20 mg of powder and then finger tapped until the powder was homogeneously scattered onto a microscopic slide. For each sample, one hundred particles were selected from different positions and measured. Particle elongation ratio (ER) and roundness (RO) were calculated using Eqs. (1) and (2) respectively:

$$\mathrm{ER} = \frac{\text{Maximum feret diameter}}{\text{Minimum feret diameter}} \quad (1)$$

$$RO = \frac{(\text{Perimeter})^2}{4 \times \pi \times \text{area}} \quad (2)$$

where the minimum and maximum Feret diameters were calculated from 16 calliper measurements at 6° intervals around the particle and "area" in Eq. (2) is the area occupied by particle images.

2.5. Scanning electron microscope (SEM)

Electron micrographs of all carrier samples were obtained using a scanning electron microscope (Philips XL 20, Eindhoven, Netherlands) operated at 15 kV. The specimens were mounted on a metal stub with double-sided adhesive tape and coated under vacuum with gold in an argon atmosphere prior to observation.

2.6. Particle size measurements

Particle size analyses were conducted by Sympatec laser diffraction particle size analyser (Clausthal-Zellerfeld, Germany) as described in details elsewhere (Kaialy et al., 2010b).

2.7. True density assessments

Ultrapycnometer 1000 (Quantachrom, USA) was employed to assess true density of salbutamol sulphate and all carrier samples under helium gas. The input gas pressure was 19 psi and the equilibrium time was 1 min.

2.8. Powder flow and porosity assessment

Bulk density (D_b) and tap density (D_t) of all carrier powders were measured as descriptors of bulk powder cohesive properties. Each carrier powder was filled in 5 mL measuring cylinder and then after recording the volume (bulk volume) the cylinder was tapped 100 times and the new volume was recorded (tapped volume). A preliminary experiment showed that 100 taps (n = 100) was sufficient to attain the maximum reduction in the volume of powder bed. D_b and D_t were calculated as powder weight over powder bulk volume (n = 0) and tap volume (n = 100) respectively. Flowability of each carrier powder was estimated by Carr's compressibility index (CI) and Hausner ratio (H) calculated using Eqs. (3) and (4) (Carr,

1965a, b; Hausner, 1967) where D_b and D_t represent bulk density and tap density respectively.

$$CI = 100 \times \frac{D_t - D_b}{D_t} \quad (3)$$

$$H_R = \frac{D_t}{D_b} \quad (4)$$

Angle of repose (α) is the most commonly used method to describe powder flowability (Kumar et al., 2004). In order to calculate (α), a pile was built by dropping 1 g of powder through a 75 mm flask on a flat surface. The height between the base where the powder was poured and the funnel tip was 3 cm. The angle of repose (α) was then calculated by the following equation:

$$\mathrm{Tan}\,\alpha = \frac{2h}{D} \quad (5)$$

where h is the height of the powder cone and D the diameter of the base of the formed powder pile. Higher CI, higher H_R, or higher α is indicative of poorer flow properties. Porosity (P) of each carrier powder was calculated using the following equation (Kumar et al., 2001)

$$P = 100 \times \left(1 - \frac{D_b}{D_t}\right) \quad (6)$$

2.9. X-ray powder diffractometery

PXRD patterns of the samples were collected on a Siemens DIFFRACplus 5000 powder diffractometer with CuKα radiation (1.54056 Å). The tube voltage and amperage were set at 40 kV and 40 mA, respectively. The monochromator slit was set at 20 mm sample size. Each sample was scanned between 5° and 40° in 2θ with a step size of 0.01° at 1 step/s. The sample stage was spun at 30 rpm. The instrument was calibrated prior to use, using a silicon standard.

2.10. Blending of salbutamol sulphate with different carriers

Each 63–90 μm sieved carrier powder was mixed with salbutamol sulphate (SS) at a ratio of 67.5:1 (w/w) in accordance with the ratio used in commercial product Ventolin™ Rotacaps™ (GSK). Powders (about 2 g) were filled in cylindrical aluminum bottle (6.5 cm diameter × 8 cm height) and blended using Turbula® mixer (Maschinenfabrik, Basel, Switzerland) for 30 min at a constant speed of 100 rpm. Five different formulations were prepared with five different carrier products and then stored in tightly sealed vials until use.

2.11. Drug content uniformity test

In order to examine drug content uniformity for different formulations after blending, minimum five aliquots (taken from random positions of each blend) of 33 ± 1.5 mg (which is the amount of powder equivalent to a unit dose) were accurately weight. Then each aliquot was dissolved in deionised water to 100 mL volumetric flask final volume and the amount of SS was analyzed using HPLC described elsewhere (Kaialy et al., 2010a). For each blend, the average drug content was calculated and the mean drug recovery (% uniformity) was expressed as a percentage to the expected theoretical dose (481 ± 22 μg). Blends homogeneity was expressed as the percentage coefficient of variation in drug content (CV, %).

2.12. Capsule filling

Each formulation blend was loaded manually into size 3 hard gelatin capsules with 33 ± 1.5 mg powder corresponding to 481 ± 22 μg of SS in each capsule as theoretical dose. Following filling, capsules were sealed in tight glass vials till used in deposition analysis.

2.13. Deposition test of Salbutamol sulphate

In vitro aerosolisation performance of SS from Aerolizer® inhaler device (supplied by Vectura, UK, and originated by Novartis, Switzerland) was determined and Multi Stage Liquid Impinger (MSLI) equipped with USP induction port (Copley scientific, Nottingham, UK) at flow rate of 92 L/min (corresponds to a pressure drop of 4 KPa across the device). The MSLI assemble and deposition experiments were performed as described by USP Pharmacopeia (2003) and explained in details elsewhere (Kaialy et al., 2010a). Several deposition parameters were used to characterize the drug aerosolisation behaviour from different formulation blends. The recovered dose (RD) was defined as the sum of the amounts of drug (μg) recovered from inhaler device with its fitted mouthpiece adaptor (I + M), induction port (IP), and all stages of the MSLI. The emitted dose (ED) was defined as the amount of drug delivered from the inhaler device, which is collected from the IP and all MSLI stages. Fine particle dose (FPD) (defined as amounts of drug particles with aerodynamic diameter ≤ 5 μm), mass median aerodynamic diameter (MMAD), and geometric standard deviation (GSD) were calculated from the interpolation of drug aerodynamic size distribution as described in details elsewhere (USP Pharmacopeia, 2003). Fine particle fraction (FPF) was calculated as the percentage of FPD to the RD. Dispersibility (DS) was calculated as the percentage of FPD to the ED. Effective inhalation index (EI) was calculated as follows:

$$EI = (EM \times FPF)^{\frac{1}{2}} \quad (7)$$

Theoretical aerodynamic diameter of SS (D_{ae}) was calculated from geometrical mean particle diameter (D_e) and particle true density (ρ) using the following equation (Velaga et al., 2004):

$$D_{ae} = D_e \times \left(\frac{\rho}{X}\right)^{0.5} \quad (8)$$

where X is shape factor for non-spherical particles which was estimated to be 1 (Hassan and Lau, 2009). The percent total recovery (RE) was calculated as the ratio of the RD to the theoretical dose (481 ± 22 μg). The percent emission (EM) was the percent ratio of the ED to RD. Impaction loss (IL) was defined as the amount of drug deposited on the IP and stage 1 of the MSLI as a percentage to the RD. A total of 5 different DPI formulation blends were investigated with 5 different carrier powders and all *in vitro* assessments were performed in triplicate.

2.14. Statistical analysis

One way analysis of variance (ANOVA) test was applied to compare mean results in this study considering P values less than 0.05 as indicative of significant difference. This test was conducted using Excel software (2007, UK). When appropriate and when ANOVA indicated significant difference, Tukey's Honestly Significant Difference (HSD) test was performed.

3. Results and discussions

3.1. Characterization of carrier particle size and morphology

Elongation ratio (ER) and roundness (RO) for different carrier particles were measured and results are shown in Fig. 1 along with representative photographs of different carrier particles. It can be seen that the particle morphologies of different carrier samples differ considerably (Fig. 1). A typical sphere (represented by two

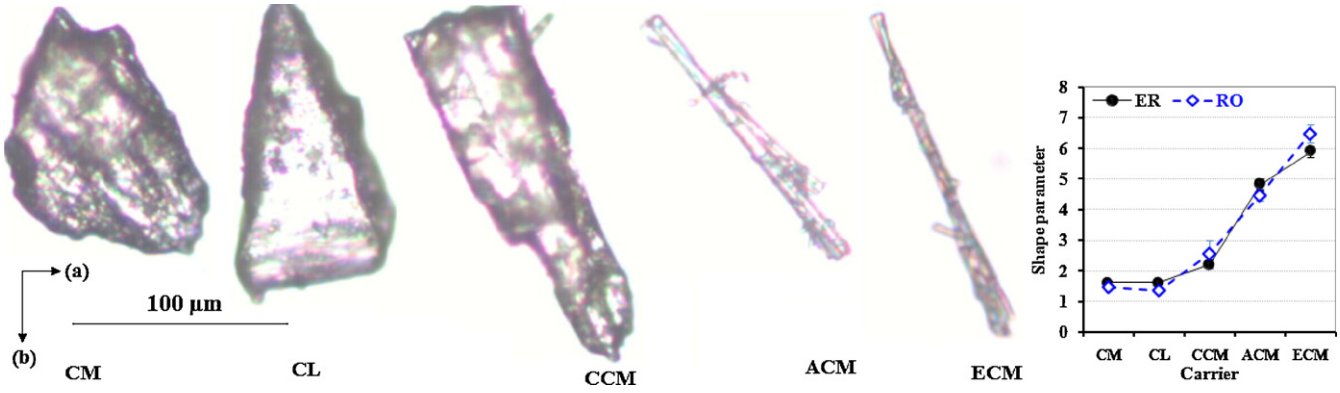

Fig. 1. Representative photographs of different carrier crystals: (CM) commercial mannitol, (CL) commercial lactose, (CCM) cooling crystallised mannitol, (ACM) acetone crystallised mannitol, and (ECM) ethanol crystallised mannitol.

dimensional circle) with surface asperities below the level of discrimination of the employed method will have ER and RO values of 1 (Larhrib et al., 1999). The ER for different carrier particles ranged from 1.62 ± 0.04 for CM to 5.89 ± 0.2 for ECM (mean $\pm$ SE, $n = 100$) (Fig. 1). Higher ER indicates that particles are more elongated and/or more irregular in shape (Allen, 1981).

RO is a second order shape property reflecting variations at particle corners (Barrett, 1980). Particles with higher particle RO is indicative of their more irregular shape and/or rougher surface. RO measurements for different carrier particles ranged from 1.36 ± 0.13 for CL to 6.49 ± 2.91 to ECM (mean $\pm$ SE, $n = 100$) (Fig. 1). Interacting carrier particles are expected to have different interparticulate forces depending on interparticulate contact area. Carrier particles with high ER and high RO values are likely to exhibit pronounced internal friction due to angular shape of the particles and thus are expected to have different aerosolisation characteristics (Zeng et al., 2001a, b).

However, the use of only shape factors may not be sufficient to study the effect of particle shape since particle shape assessments using microscopic image analysis can be influenced by particle orientation and contact hindering the accuracy of the technique (Hassan and Lau, 2009). Therefore, shape and surface morphology of all carrier particles was qualitatively examined by SEM. Representative SEM electrographs for different carriers are shown in Fig. 2. It can be seen that carrier samples varied considerably in terms of particle size, shape, and surface morphologies. SEM

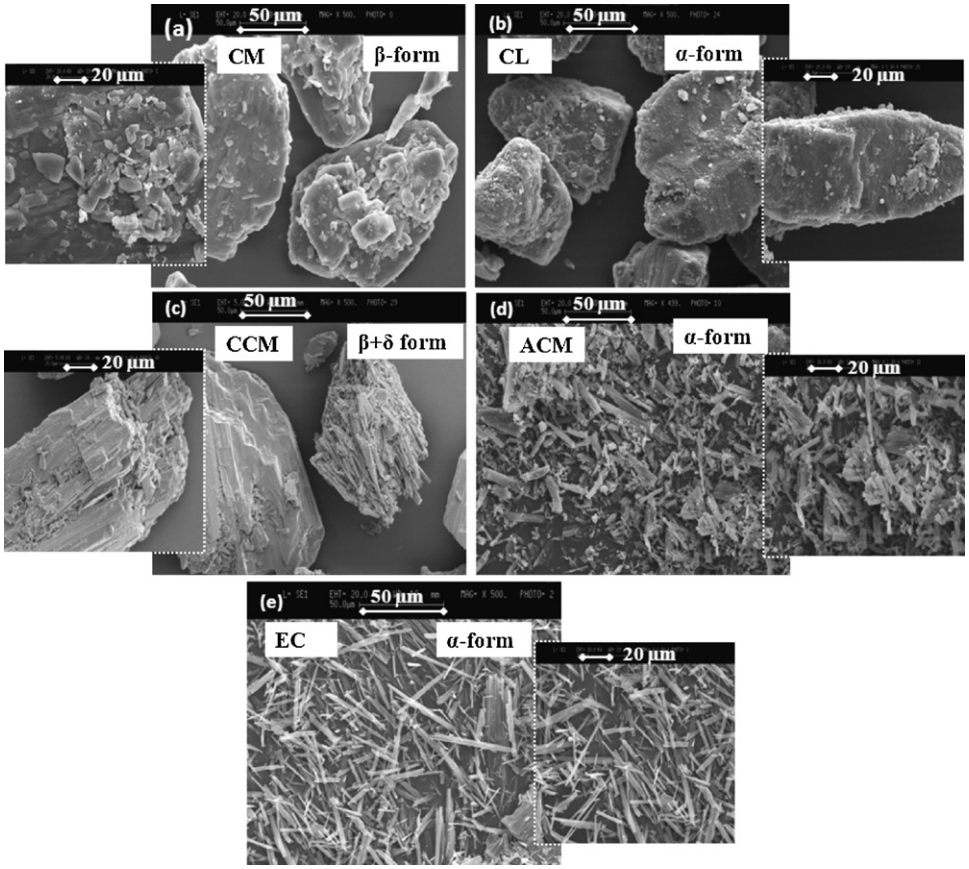

Fig. 2. SEM micrographs of different 63–90 µm sieved carriers: (CM) commercial mannitol, (CL) commercial lactose, (CCM) cooling crystallised mannitol, (ACM) acetone crystallised mannitol, and (ECM) ethanol crystallised mannitol.

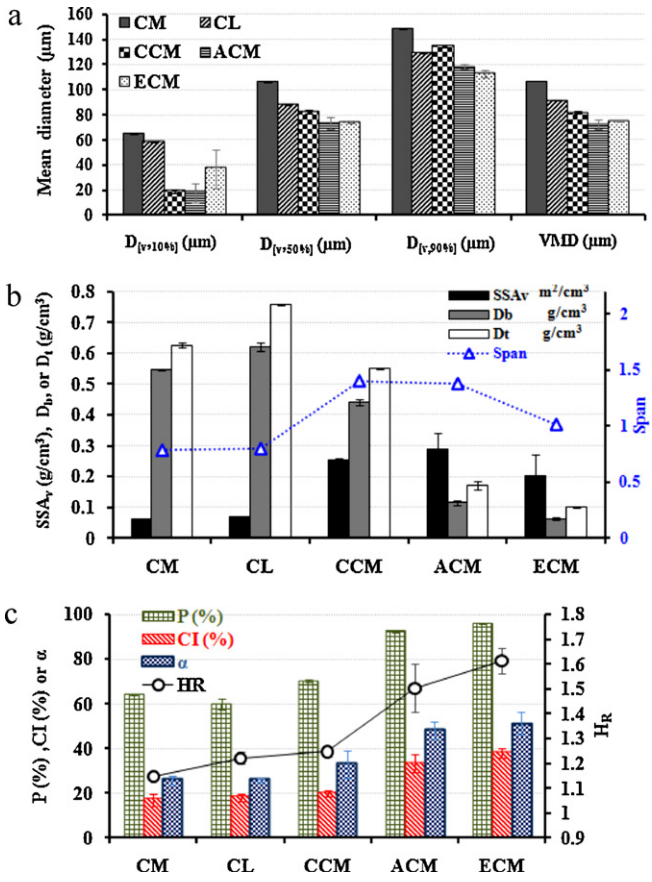

Fig. 3. Mean particle size at 10% ($D_{[v,\,10\%]}$), 50% ($D_{[v,\,50\%]}$), 90% ($D_{[v,\,90\%]}$) volume distribution, volume mean diameter (VMD) (a); volume specific surface area (SSAv), bulk density (D_b), tap density (D_t), span (b); porosity (P), Carr's index (CI), angle of repose (α), and Hausner ratio (H_R) (c) of different 63–90 μm sieved carriers: commercial mannitol (CM), commercial lactose (CL), cooling crystallised mannitol (CCM), acetone crystallised mannitol (ACM), and ethanol crystallised mannitol (ECM) (mean ± SD, $n \geq 3$).

micrographs showed the typical shape reported in literature for CM (angular particles with surface asperities) (Fig. 2a; Tang et al., 2009; Ansari and Stepanek, 2008; Rajniak et al., 2007) and CL (tomahawk shape) (Fig. 2b; Van Kreveld and Michaels, 1965; Raghavan et al., 2000). CCM sample was observed as particles with surface protuberances forming angular edges (Fig. 2c). In line with ER and RO values obtained by image analysis (Fig. 1), ACM and ECM particles were more elongated and more irregular (deformed) in shape than both CM and CL (Fig. 2d and e). Also, it is evident that ACM and ECM particles are less homogenous (less uniform) with varying degrees of agglomeration (Fig. 2d and e). CM, CL, and CCM particles showed wrinkled surface topography with high degree of roughness and asperities (Fig. 2a–c). In contrast, ACM and ECM samples consist of particles with smoother surface and higher amounts of fines (Fig. 2d and e).

In fact, particle shape and size determinations are dependent on each other since assumptions about particle size should be made in order to define particle shape and vice versa. Particle size distributions (PSD) for all carrier powders were measured and the data are shown in Fig. 3. It can be seen that despite all samples were sieved carefully into the same size fraction intended for this study (63–90 μm); identical PSDs for different carrier powders could not be obtained. Statistically, the PSD [in terms of mean particle size at 10% ($D_{[v,\,10\%]}$), 50% ($D_{[v,\,50\%]}$), 90% ($D_{[v,\,90\%]}$) volume distribution and volume mean diameter (VMD)] for different carriers were in the following rank order (Fig. 3a): CM > CL > CCM > ACM ≈ ECM. These differences in carrier particle size could be, in part, attributed to

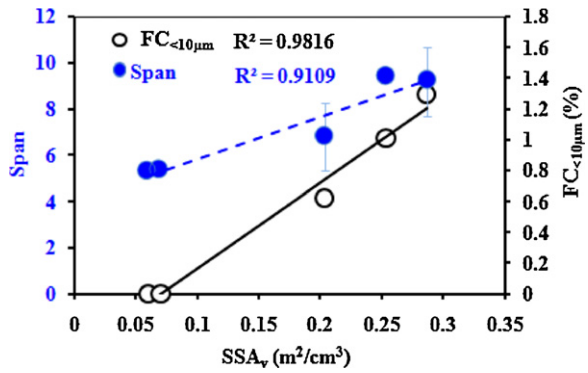

Fig. 4. Relationships between carrier volume specific surface area (SSAv), span, and fine particles content FC < 10.5 μm for different carriers (mean ± SD, $n = 3$).

differences in particle shape as, after sieving; PSD is more related to particle breadth which is considerably different from VMD measured by laser diffraction. In case of CM, CL and CCM samples, particle VMD might have been overestimated by laser diffraction due to their rougher particle surface morphology (Fig. 2; Chew and Chan, 2001). Also, low accuracy in terms of PSD is expected in case of ACM and ECM particles due to their needle-like shape (Fig. 2; Tinke et al., 2008; Neumann and Kramer, 2002).

Unlike CM and CL, which contain no fine carrier particles (FC < 10 μm), small amounts of "intrinsic" (not added) fines could be detected in case of CCM (6.7 ± 0.3%), ACM (8.6 ± 2.0%) and ECM (4.1 ± 3.0%). Correlating well with SEM micrographs, CM and CL showed considerably ($P < 0.05$) smaller span values (calculated as $D_{[v,\,90\%]} - D_{[v,\,10\%]}/D_{[v,\,50\%]}$) than ACM and ECM samples (Fig. 3b) indicating their more homogeneous PSD. This could be attributed to heterogeneous growth of the crystals in case of CCM, ACM and ECM resulting in wider PSD. Volume specific surface area (SSA_v) of different carrier particles were in the following rank order: CM < CL < ECM < CCM < ACM (Fig. 3b). In agreement with previous studies (Sethuraman and Hickey, 2002), Fig. 4 shows higher SSA_v for carriers with wider size distribution (higher span) (linear, $r^2 = 0.9109$) and higher fines content (FC < 10 μm) (linear, $r^2 = 0.9816$).

3.2. Assessment of carrier density and flowability

True density (D_{true}), bulk density (D_b), and tap density (D_t) of different carrier particles were measured. D_{true} for CM and CL (Table 1) were similar to true density values reported in literature (1.514 g/cm³ and 1.545 g/cm³ for CM and CL, respectively (Rowe et al., 2003)). CCM showed the smallest D_{true} while ACM and ECM showed similar D_{true} ($P > 0.05$) (Table 1). Unlike D_{true}, which is a particle characteristic property, D_b and D_t are powder characteristic properties. Statistically, D_b and D_t for different carrier powders were in the following rank order: CL > CM > CCM > ACM > ECM (Fig. 3b). Carrier powder porosity (P) has significantly increased

Table 1
True density (D_{true}) (mean ± SD, $n \geq 3$), flow character, and polymorphic form of different carrier products: commercial mannitol (CM), commercial lactose (CL), cooling crystallised mannitol (CCM), acetone crystallised mannitol (ACM), and ethanol crystallised mannitol (ECM).

Carrier product (63–90 μm)	D_{true} (g/cm³)	Flow character	Polymorphic form
CM	1.52 (0.00)	Good–fair	β
CL	1.55 (0.05)	Good–fair	α
CCM	1.48 (0.01)	Fair	$\beta + \delta$
ACM	1.51 (0.01)	Poor	α
ECM	1.51 (0.00)	Very poor	α

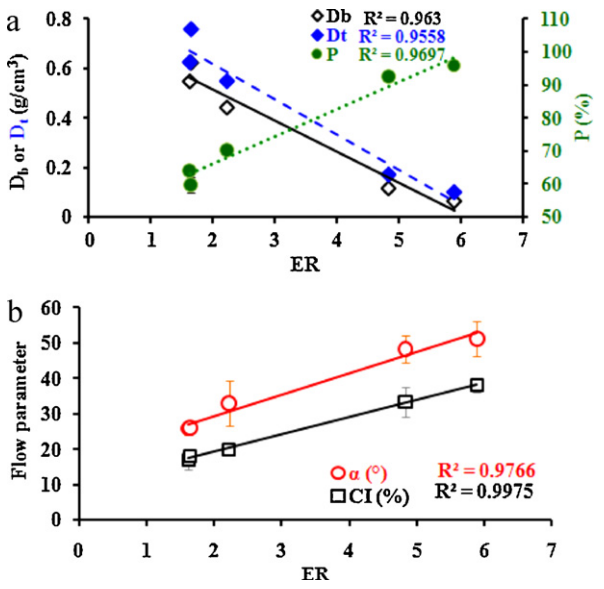

Fig. 5. Relationships between elongation ratio (ER) and (◊) carrier bulk density (D_b), (♦) tap density (D_t), (●) porosity (P) (a); (○) angle of repose, and (□) Carr's index (CI) (b) for different carriers (mean ± SD, $n \geq 3$).

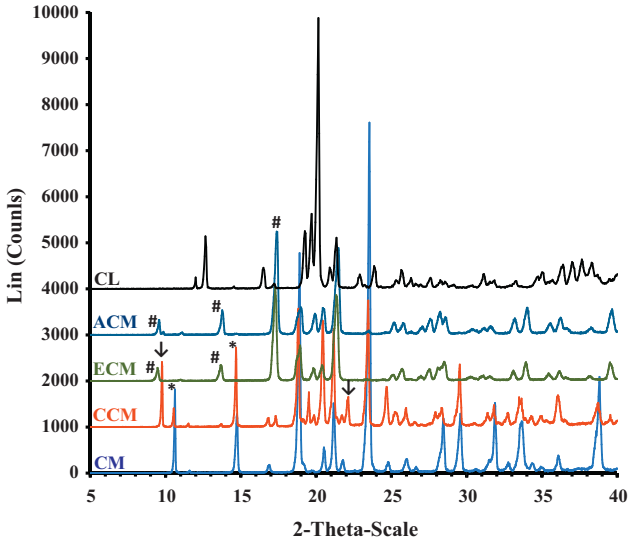

Fig. 6. XRPD patterns of different carriers: (CM) commercial mannitol, (CL) commercial lactose, (CCM) cooling crystallised mannitol, (ACM) acetone crystallised mannitol, and (ECM) ethanol crystallised mannitol. *: β-mannitol specific peak, #: α-mannitol specific peak, ↓: δ-mannitol specific peak, •: α-lactose-monohydrate specific peak.

from 59.76 ± 2.28% for CL to 95.86 ± 0.18% for ECM (Fig. 3c). Comparing all ER, D_b, and P values for different carriers showed that carriers with higher ER have smaller D_b (linear, $r^2 = 0.963$), smaller D_t (linear, $r^2 = 0.9558$), and higher P (linear, $r^2 = 0.9697$) (Fig. 5a). This could be explained by high interlocking ability (as confirmed by Fig. 2) and high void spaces between elongated particles (unisometric particles). In fact, a carrier with smaller D_b and higher P (due to higher particle ER) is indicative that this carrier has lower Van der Waal interparticulate forces as a result of decreased number of average contact points between particles (Edwards et al., 1997; Fukuoka and Kimura, 1992; Neumann, 1967).

In order to obtain valid flowability data for different samples, Carr's index (CI), Hausner ratio (H_R), and angle of repose (α) for all carrier powders were measured and shown in Fig. 3c. It can be seen that CM, CL, and CCM powders have considerably ($P < 0.05$) smaller CI, smaller H_R, and smaller α than ACM and ECM powders (Fig. 3c). These differences reflect different interparticulate forces and flow characteristics among carrier powders (Table 1). In fact, this was understandable considering morphological differences between carrier particles (Figs. 1 and 2). Direct linear relationships were obtained when plotting carrier particle ER against α ($r^2 = 0.9766$) or CI ($r^2 = 0.9975$) (Fig. 5b), indicating poorer flowability for carriers with higher particle ER.

3.3. Carrier solid state characterization

Different carrier samples were analysed using Powder X-ray diffraction (PXRD) and all patterns are presented in Fig. 6. All samples were highly crystalline in nature. Mannitol is known to exist in three anhydrous polymorphic forms and one hydrated form (Campbell Roberts et al., 2002). The peaks in the PXRD patterns of the mannitol samples were compared with the reference patterns of pure α-, β-, and δ-mannitol (Yoshinari et al., 2002; Yu et al., 1999; Hawe and Frie, 2006; Burger et al., 2000; Debord et al., 1987; Jones and Lee, 1970). CM was confirmed to be β-form (most stable form at ambient conditions) with characteristic PXRD peaks at 10.56° and 14.5° 2θ whereas ACM and ECM products were α-forms with diagnostic peaks at 9.57°, 13.79°, and 17.2° 2θ (Fig. 6). CCM showed diagnostic peaks of both β-form (at 10.56° and 14.5° 2θ) and δ-form (at 9.7° and 22.2° 2θ) (δ-mannitol is metastable form, stable for 5 years in dry atmosphere at 25 °C) (Sharma and Kalonia, 2004; Walter-Levy, 1968). CL showed the PXRD pattern of α-lactose-monohydrate which has been well documented by previous studies (Haque and Roos, 2005) having specific diagnostic peaks at 12.5°, 16.4°, and 20° 2θ. In conclusion, CM product was β-form, CL product was α-form, ACM and ECM products were α-forms, while CCM crystallised as mixtures of α-form and δ-form.

3.4. Drug–carrier formulation assessments

3.4.1. Drug content uniformity

Mean drug potency (% uniformity to theoretical dose: 481 ± 22 μg) and coefficient of variation (% CV) of drug content obtained from formulation blends containing different carriers were assessed and shown in Fig. 7. Uniformity (%) of all formulation blends fall within the acceptable range of nominal dose ± 10% for SS in DPI dosage forms. In general, carriers with higher ER produced higher ($P < 0.05$) % uniformity of SS within SS-carrier formulations (Fig. 7). CV (%) of SS content varied from 8.0% to 10.9% for different blends. In fact, variations in the drug content homogeneity (expressed as % CV) for DPI formulations containing different carriers were expected, as different powders may require different mixing conditions (Staniforth et al., 1982). Nevertheless, as blending has a significant effect on drug–carrier

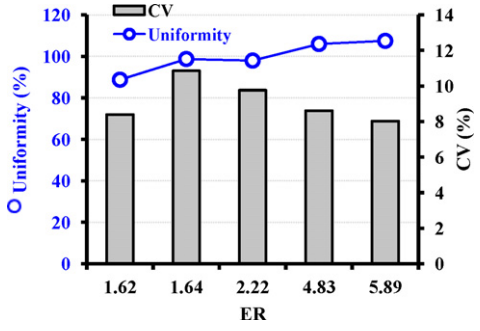

Fig. 7. (○) Uniformity and (■) coefficient of variation (CV) of salbutamol sulphate content obtained from formulations containing carriers with different elongation ratio (ER).

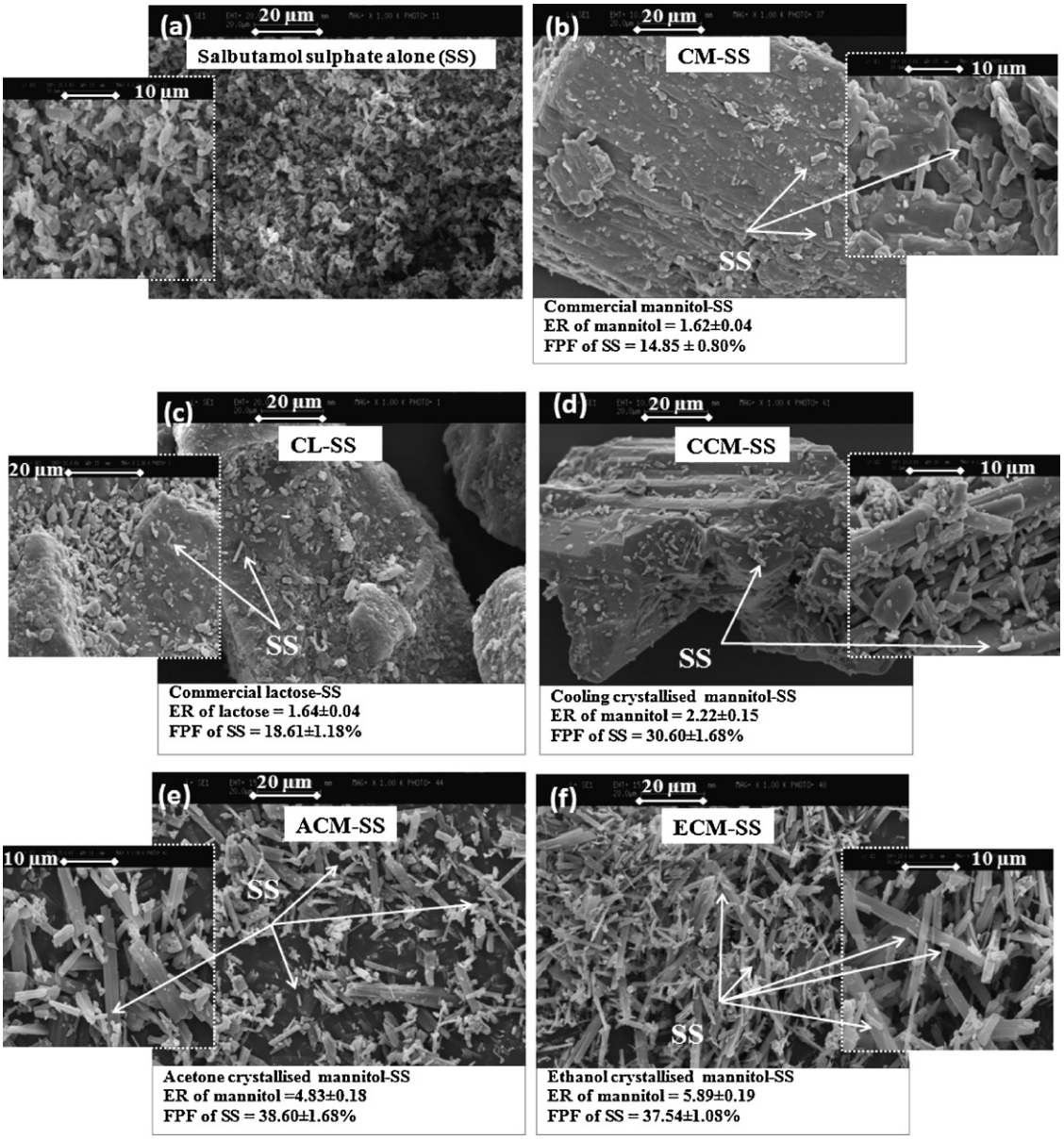

Fig. 8. SEM micrographs of formulation blends containing salbutamol sulphate with different 63–90 μm sieved carrier particles: (CM) commercial mannitol, (CL) commercial lactose, (CCM) cooling crystallised mannitol, (ACM) acetone crystallised mannitol, and (ECM) ethanol crystallised mannitol. ER: elongation ratio, FPF: fine particle fraction (mean ± SE).

interactions (interparticulate forces) (Iida et al., 2000; Dickhoff et al., 2006), and for the comparison purpose of this study, blending process for all formulations was kept consistent.

3.4.2. Evaluation of drug–carrier formulations by SEM

SEM micrographs showed the typical rod-like particles of micronized SS (Fig. 8a; Raula et al., 2007; Young and Price, 2004; Elajnaf et al., 2006) as aggregates. However, in case of drug–carrier formulations, SS appeared to be adhered to carrier particles as individual particles (Fig. 8b–f). This confirms the formation of drug–carrier interactive mixtures typical for DPI systems. By observing surface topography of different carrier particles using higher magnifications, macroscopic depressions and cavities could be observed in case of CM (Fig. 8b), CL (Fig. 8c), and CCM (Fig. 8d). These macroscopic depressions might cause drug entrapment within carrier surface leading to poor drug–carrier detachment upon inhalation (Ganderton and Kassem, 1992). On the other hand, it is evident that ACM and ECM particles have flatter and smoother surfaces (Fig. 8e and f). To a certain point, the increase in surface flatness of carrier particles is expected to facilitate drug re-dispersion during aerosolisation process (due to decreased number of drug particles remained on the macroscopic depressions on carrier surface following inhalation (Iida et al., 2003)). Morphologically, it was noted that ACM and ECM particles have higher amounts of drug particles attached on their surface (Fig. 8e and f). This could be related to higher SSA_v for ACM and ECM particles (Kawashima et al., 1998) as it is evident in Fig. 8e and f and further quantitatively supported by laser diffraction as discussed previously (Fig. 3b).

3.4.3. In vitro aerosolisation studies

The deposition patterns of SS from different formulation blends are shown in Fig. 9. It can be seen that different formulations produced different SS deposition profiles. SS deposited preferably on MSLI-stage 1, representing the upper airway regions, irrespective of the formulation/carrier whereas all formulations exhibited minimal SS deposition on the MSLI-filter (Fig. 9I).

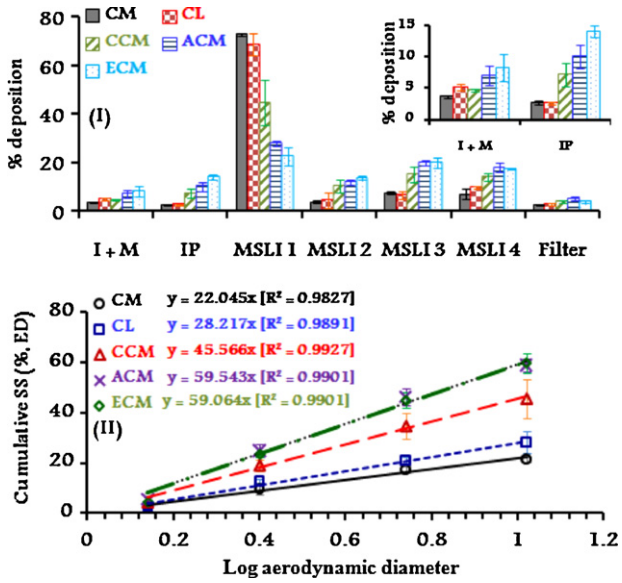

Fig. 9. Amounts of salbutamol sulphate (SS) deposited on inhaler with mouthpiece adaptor (I + M), induction port (IP), and different MSLI stages (I), and aerodynamic particle size distribution of SS (II) obtained from formulation blends containing commercial mannitol (CM), commercial lactose (CL), cooling crystallised mannitol (CCM), acetone crystallised mannitol (ACM), and ethanol crystallised mannitol (ECM).

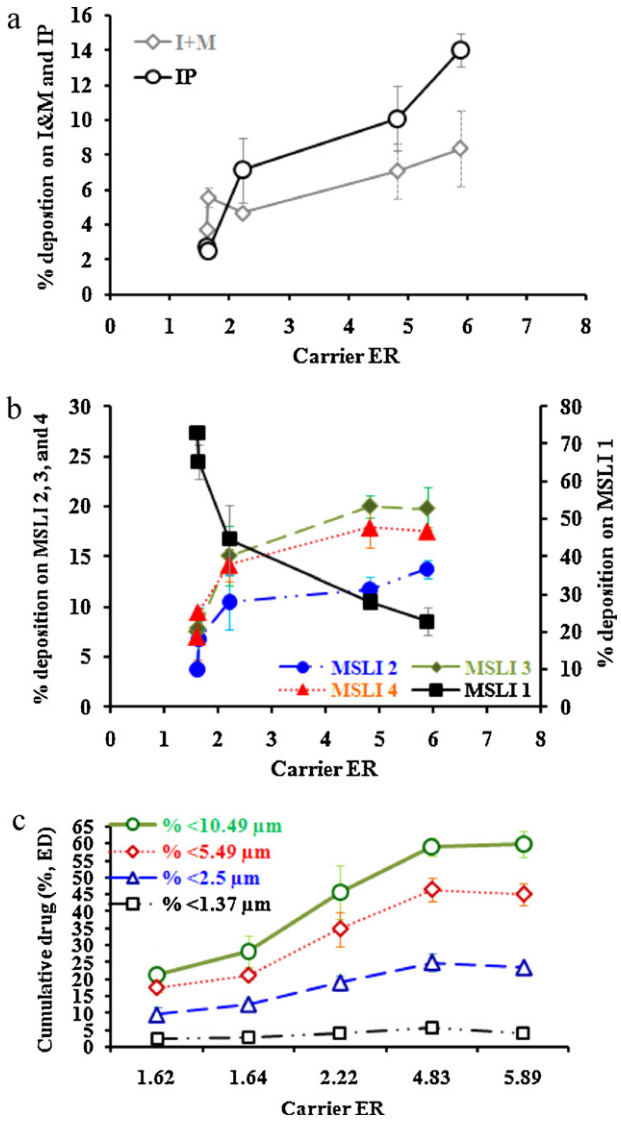

Fig. 10. Amounts of salbutamol sulphate (%, emitted dose) deposited on inhaler with mouthpiece adaptor (I + M), induction port (IP) (a), various MSLI stages (b), and cumulative amounts of SS with aerodynamic diameter <10.5 μm, <5.5 μm, <2.5 μm, and <1.4 μm in relation to carrier elongation ratio (ER) (mean ± SD, $n = 3$).

Amounts of SS remained in inhaler with mouthpiece adaptor (I + M) (drug residue or drug loss) has considerably ($P < 0.05$) increased from 3.7 ± 0.2% for CM blend to 8.4 ± 2.2% for ECM blend (Fig. 9I). Amounts of SS deposited on IP (resembling the human oropharynx) have significantly increased from 2.5 ± 0.1% for SS–CL formulation to 14.02 ± 0.93% for SS-ECM formulation (Fig. 9I). Higher amounts of drug deposited on IP is considered disadvantageous for DPI systems, as increased amounts of drug deposited on the oropharyngeal region might increase the potential for local side effects.

In contrast to SS–CM and SS–CL formulations, SS–ACM and SS–ECM formulations delivered the largest proportion of SS to MSLI stages 2, 3, and 4 and the least amounts to MSLI stage 1 (Fig. 9I). Aerodynamic PSD of SS obtained from different formulations is shown in Fig. 9II. It can be seen that linear aerodynamic PSD curves with different slops were obtained for all different formulations. Apparently, the slope of these curves reflects the tendency of drug particles to penetrate deeper into lower lung airways. These slope values (named constant *K*) obtained from aerodynamic PSD for all tested formulations are listed in Table 2. These findings indicate that the efficiency of SS particles detachment from carrier surface was dependent on the carrier type employed within each formulation.

Fig. 10 shows the effect of carrier ER on SS deposition profiles. It can be observed that, in general, carriers with higher ER produced higher amounts of drug remained in I + M and/or deposited on IP (Fig. 10a). This could be due to the poor flowability and high cohesive nature of carriers with higher ER, as discussed earlier (Fig. 5b). Poor flowability of carriers with higher ER results in poor powder fluidization (dispersion) upon inhalation and consequently higher amounts of powder retained by the plastic gird of the Aerolizer® and/or the aggregates deposited on the throat (IP) (Rabbani and Seville, 2005; Seville et al., 2002; Begat et al., 2004).

Generally, carriers with higher ER deposited smaller amounts of SS on MSLI stage 1 while higher amounts on MSLI stages 2, 3, and 4 (Fig. 10b). In Fig. 10c, cumulative amounts of SS with aerodynamic size less than 10.49 μm, 5.49 μm, 2.5 μm, and 1.37 μm

Table 2
Recovered dose (RD), emitted dose (ED), recovery (RE), emission (EM), impaction loss (IL), dispersibility (DS), fine particle dose (FPD), fine particle fraction (FPF), effective inhalation index (EI), and constant K of salbutamol sulphate obtained from DPI formulations containing commercial mannitol (CM), commercial lactose (CL), cooling crystallised mannitol (CCM), acetone crystallised mannitol (ACM), and ethanol crystallised mannitol (ECM) (mean ± SD, $n = 3$).

Carrier	RD (μm)	ED (μm)	RE (%)	EM (%)	IL (%)	DS (%)	FPF (%)	EI (%)	FPD (μg)	Constant *K*
CM	381.5 ± 8.3	367.3 ± 8.8	79.3 ± 1.7	96.3 ± 0.2	75.7 ± 0.7	15.4 ± 1.1	14.8 ± 1.1	37.8 ± 1.5	56.7 ± 5.6	22.1 ± 1.6
CL	317.0 ± 5.1	299.4 ± 6.6	65.9 ± 1.0	94.5 ± 0.6	67.8 ± 4.7	19.7 ± 1.9	18.6 ± 1.7	41.9 ± 1.8	59.0 ± 4.3	28.2 ± 3.0
CCM	469.5 ± 30.2	447.6 ± 28.9	97.6 ± 6.3	95.3 ± 0.2	51.7 ± 7.4	31.7 ± 4.9	30.3 ± 4.7	53.6 ± 4.3	142. 8 ± 29.4	45.6 ± 7.1
ACM	426.6 ± 25.3	396.7 ± 29. 9	88.7 ± 5.3	92.9 ± 1. 6	38.1 ± 2.0	41.5 ± 2.6	38.6 ± 2.9	59.9 ± 2.7	165.0 ± 2.0	59.5 ± 3.6
ECM	464.7 ± 22.6	425.6 ± 15.8	96.6 ± 4.7	91.7 ± 2.2	36.7 ± 4.2	41.0 ± 2.6	37.5 ± 1. 7	58.6 ± 1.3	174.3 ± 9.1	59.1 ± 3.8

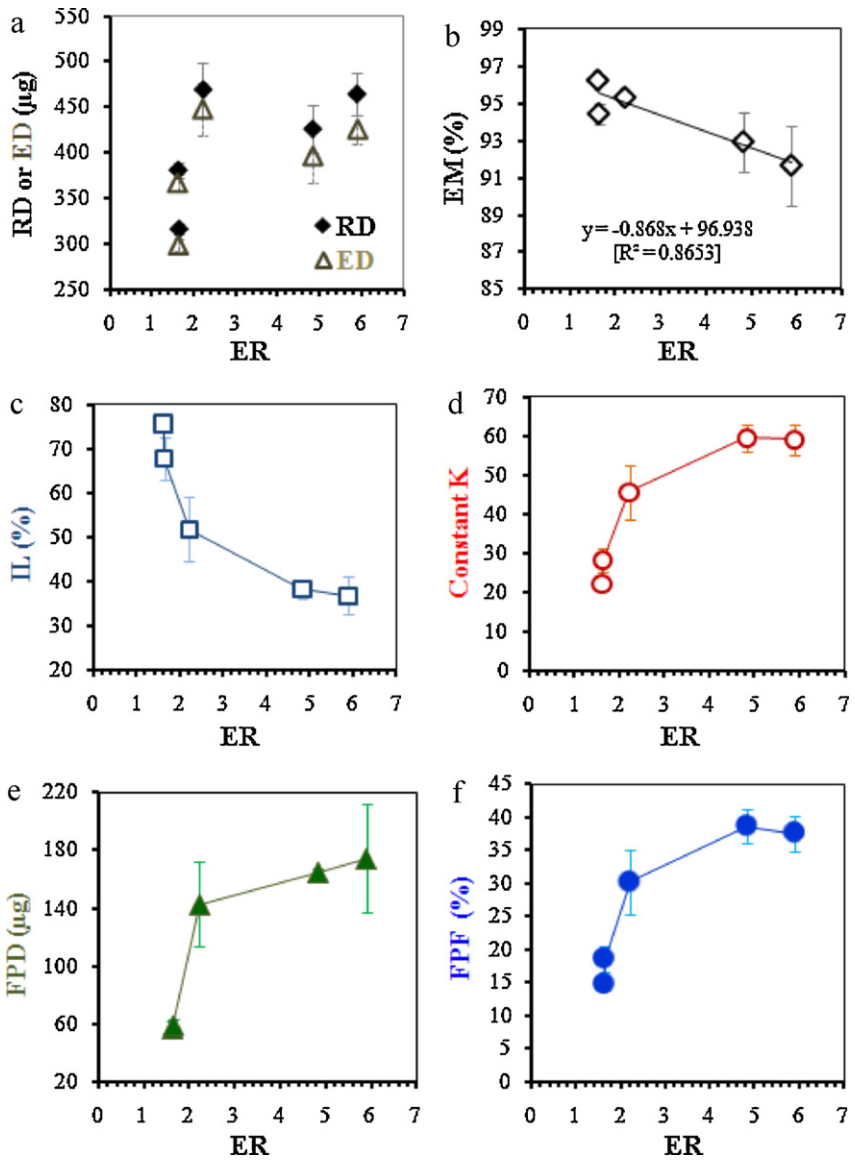

Fig. 11. Relationships between carrier elongation ratio (ER) and salbutamol sulphate (♦) recovered dose (RD), (Δ) emitted dose (ED) (a); (◊) emission (EM) (b), (□) impaction loss (IL) (c), (○) constant *K* (d), (▲) fine particle dose (FPD) (e), and (●) fine particle fraction (FPF) (f) when aerosolised from Aerolizer® through MSLI at 92 l/min (mean ± SD, $n = 3$).

were plotted against carrier ER. It is clear that, generally, higher amounts of SS with aerodynamic diameter less than 10.49 μm, 5.49 μm, and 2.5 μm were produced by using carriers with higher ER. This indicates that SS particles adhered to carriers with higher ER were aerodynamically "more efficient" than drug particles adhered to carriers with smaller ER. However, when carrier ER increased from 4.83 to 5.89, the amounts of cumulative SS did not change significantly ($P > 0.05$) (Fig. 10c).

Different formulations produced different ($P < 0.05$) recovered dose (RD), emitted dose (ED), recovery (RE) and emission (EM) of SS according to carrier used (Table 2). Except for SS–CL formulation, RE for all formulations falls within the acceptable range of 75–125% (Byron et al., 1994) (Table 2). Differences in RD, ED, RE and EM could be attributed to different carriers employed within different formulations. Generally, carriers with higher ER produced higher RD and ED of SS upon inhalation (Fig. 11a). This could be ascribed to less drug–carrier mechanical interlocking in case of carriers with higher ER leading to increased drug–carrier detachment upon inhalation. It can be seen that, compared to CM and CL, ACM and ECM carriers produced higher RDs and EDs of SS but lower EMs ($P < 0.05$) (Table 1). In fact, RD and ED are aerosolisation properties while EM is more related to powder flowability (Smyth and Hickey, 2005; Jiang et al., 2005; Murakoshi et al., 2005). Fig. 11b shows that carriers with higher ER produced smaller EM of SS upon inhalation (linear, $r^2 = 0.8653$). This could be attributed to poor flowability for carriers with higher ER (Fig. 5b) which is expected to negatively affect powder outflow during inhalation (Iida et al., 2001).

In DPIs, drug aerodynamic diameter is an important measure that determines its deposition site in the lungs, and thereby, the success of inhalation therapy. In this study, SS showed geometric mean diameter (D_e) and theoretical aerodynamic diameter (D_{ae}) of 1.8 ± 0.3 μm and 2.1 ± 0.3 μm (mean ± SD, $n = 3$), respectively. In fact, higher D_{ae} of SS compared to D_e was expected as SS have D_{true} higher than 1 (1.39 ± 0.01 g/cm^3). All formulations produced similar ($P > 0.05$) mass median aerodynamic diameter (MMAD) (3.21 ± 0.18 μm) and similar geometric standard deviation (GSD) (2.15 ± 0.04) of SS (mean ± SD). However, this similarity does not necessarily indicate similar drug aerosolisation efficiency (Martonen et al., 1992). MMAD for SS (3.21 ± 0.18 μm) was significantly higher than D_{ae} (1.8 ± 0.3 μm) which could be ascribed to

cohesion (aggregation) between SS particles in dry state (Fig. 8a; Bosquillon et al., 2004) and rod-shape nature of SS particles (Fig. 8a; Bosquillon et al., 2001).

Impaction loss (IL) of SS obtained from all formulations is listed in Table 2. In theory, it can be assumed that IL refers to the amounts of drug that is still adhered to the carrier surface and has not been liberated during inhalation. By comparing different formulations, carriers with higher ER produced smaller IL of SS (Fig. 11c). This confirms that drug particles blended with carriers with higher ER were easier to detach from carrier surfaces than drug particles blended with carriers with smaller ER. Drug dispersibility (DS) ranged from $15.4 \pm 1.1\%$ for SS–CM formulation to $41.5 \pm 2.6\%$ for SS-ACM formulation whereas fine particle dose (FPD) varied between $56.7 \pm 5.6\ \mu g$ for SS–CM formulation and $174.3 \pm 9.1\ \mu g$ for SS–ECM formulation (Table 1).

In theory, according to D_e, D_{ae}, and/or MMAD, all SS particles are supposed to deposit on peripheral alveolar airway regions (Mitchell and Nagel, 2003; Stahlhofen et al., 1980) giving fine particle fraction (FPF) of 100%. Nevertheless, different formulations produced different FPFs ranging between $14.8 \pm 1.1\%$ for SS–CL formulation and $38.6 \pm 2.9\%$ for SS–ACM formulation (Table 2). In fact, in drug–carrier DPI systems, two consequent steps are crucial to achieve good inhalation performance. First step is the emission of small drug particles adhering to large carrier particles from the capsule and inhalation device, denoted by EM deposition parameter. Second step is drug separation from the emitted carrier particles (drug re-dispersion or drug–carrier de-aggregation), which could be assessed by FPF deposition parameter. However, by comparing the formulations in the study, it can be concluded that there is no apparent relationship between EM and FPF (Table 2). For an ideal DPI, effective inhalation index (EI) (which is related to both EM and FPF) should be 100% (Hino et al., 1998; Nakate et al., 2004). In this study, EI for SS was ranged between $37.80 \pm 1.49\%$ for SS–CM formulation to $59.88 \pm 2.65\%$ for SS–ACM formulation (Table 2).

FPD and Constant K produced by different formulations were in the following rank order according to carrier type: CM < CL < CCM < ACM ≈ ECM. Higher FPD and constant K indicate higher amounts of SS deposited on lower airways (which is preferred in case of SS (Price and Clissold, 1989)). It can be noticed that there is a wide variation in FPD and constant K measurements in case of SS–CCM formulation (Table 2). That could be due to high variability in physical properties of CCM sample in terms of particle shape, size, and crystal form as discussed previously.

All variations in SS aerosolisation efficiency between different formulations could be attributed to different carrier products as the same batch of drug was used in all blends. Differences in carrier shape are likely to affect drug aerosolisation performance (Hickey et al., 1992; Lippmann and Timbrell, 1990). In this study, carriers with higher ER produced higher constant K (Fig. 11d), higher FPD (Fig. 11e), and higher FPF (Fig. 11f) of SS upon inhalation indicating their better inhalation performance. This could be ascribed to enhanced drug–carrier deaggregation as a result of less stable contact area in case of elongated particles (Otsuka et al., 1988). Also, by using carriers with higher ER, carrier particles become more potential for enhanced DPI performance in terms of higher SSA_v (Fig. 3b; Cline and Dalby, 2002), higher porosity (Fig. 3c; Vanbever et al., 1999), and higher amounts of fines (Islam et al., 2004). However, statistical analysis showed that ACM ($ER = 4.83 \pm 0.18$) and ECM ($ER = 5.89 \pm 0.19$) carriers produced similar FPF for SS. This suggests an optimal carrier ER above which any further increase in carrier ER does not seem to enhance DPI inhalation performance. Finally, it is known that carrier polymorphic form has an important effect on DPI drug–carrier interactions due to its effect on particle surface free energy (Traini et al., 2008). Comparing the aerosolisation behaviour of different mannitol carrier particles investigated in this study suggested that α-mannitol carriers produced better aerosolisation performance than β-mannitol.

4. Conclusions

This report provided, for the first time, systemic comparison of several DPI formulations with increasing carrier ER up to ~6.To a certain point ($ER \approx 5$), carriers with higher ER produced higher amounts of drug delivered to lower airway regions. However, it was proved that the higher the carrier ER the poorer the flowability, the higher the amounts of drug loss, and the higher the amounts of drug deposited on throat which are all considered disadvantageous in DPI systems. Clearly, achieving control of drug aerosolisation performance requires full understanding of all parameters that are known to influence drug particle, carrier particles, and drug–carrier interactions. The present study showed that mannitol particles crystallised from either acetone or ethanol (α-mannitol) showed the best aerosolisation performance whereas poorest aerosolisation performance was obtained from grounded mannitol (β-mannitol). Unfortunately, studying the effect of only one property with keeping the other parameter/property on aerosolisation performance is practically very challenging as these properties are related to each other. Despite that the use of elongated carrier particle produced improved DPI performance; further work is required to investigate the effect of carrier ER in relation to drug ER.

Acknowledgements

Waseem Kaialy thanks Ian Slipper, School of Science, University of Greenwich for taking SEM images and Steve Ingham, Pharmacy Teaching Manager, King's College London for his help with particle shape analysis. Alhalaweh and Velaga thank the Kempe Foundation (Kempestiftelserna) for an instrumentation grant.

References

Allen, T., 1981. Particle Size Measurement, 4th ed. Chapman and Hall, Westminister, London, 128–144.
Ansari, M.A., Stepanek, F., 2008. The effect of granule microstructure on dissolution rate. Powder Technol. 181, 104–114.
Barrett, P.J., 1980. The shape of rock particles, a critical review. Sedimentology 27, 291–303.
Begat, P., Morton, D.A.V., Staniforth, J.N., Price, R., 2004. The cohesive–adhesive balances in dry powder inhaler formulations. I. Direct quantification by atomic force microscopy. Pharm. Res. 2, 1591–1597.
Bell, J.H., Hartley, P.S., Cox, J.S.G., 2006. Dry powder aerosols. I. A new powder inhalation device. J. Pharm. Sci. 60, 1559–1564.
Berard, V., Lesniewska, E., Andres, C., Pertuy, D., Laroche, C., Pourcelot, Y., 2002. Dry powder inhaler: influence of humidity on topology and adhesion studied by AFM. Int. J. Pharm. 232, 213–224.
Bosquillon, C., Lombry, C., Preat, V., Vanbever, R., 2001. Comparison of particle sizing techniques in the case of inhalation dry powders. J. Pharm. Sci. 90, 2032–2041.
Bosquillon, C., Rouxhet, P.G., Ahimou, F., Simon, D., Culot, C., Préat, V., Vanbever, R., 2004. Aerosolization properties, surface composition and physical state of spray-dried protein powders. J. Control. Release 99, 357–367.
Burger, A., Henck, J.O., Hetz, S., Rollinger, J.M., Weissnicht, A.A., Stöttner, H., 2000. Energy/temperature diagram and compression behavior of the polymorphs of D-mannitol. J. Pharm. Sci. 89, 457–468.
Byron, P.R., Kelly, E.L., Kontny, M.J., Lovering, E.G., Poochikian, G.K., Sethi, S., 1994. Recommendations of the USP advisory panel on aerosols on the USP general chapters on aerosols (601) and uniformity of dosage units (905). Pharm. Forum 20, 7477–7505.
Byron, P.R., Jashnam, R., 1990. Efficiency of aerosolization from dry powder blends of terbutaline sulfate and lactose NF with different particle-size distributions. Pharm. Res. 7, 81.
Campbell Roberts, S.N., Williams, A.C., Grimsey, I.M., Booth, S.W., 2002. Quantitative analysis of mannitol polymorphs. X-ray powder diffractometry – exploring preferred orientation effects. J. Pharm. Biomed. Anal. 28, 1149–1159.
Carr, R.L., 1965b. Classifying flow properties of solids. Chem. Eng. 72, 169–172.
Carr, R.L., 1965a. Evaluating flow properties of solids. Chem. Eng. 72, 163–168.
Chew, N.Y.K., Chan, H.K., 2001. Use of solid corrugated particles to enhance powder aerosol performance. Pharm. Res. 18, 1570–1577.

Cline, D., Dalby, R., 2002. Predicting the quality of powders for inhalation from surface energy and area. Pharm. Res. 19, 1274–1277.
Debord, B., Lefebvre, C., Guyot-Hermann, A.M., Hubert, J., Bouche, R., Cuyot, J.C., 1987. Study of different crystalline forms of mannitol: comparative behaviour under compression. Drug. Dev. Ind. Pharm. 13, 1533–1546.
Dickhoff, B.H.J., de Boer, A.H., Lambregts, D., Frijlink, H.W., 2006. The effect of carrier surface treatment on drug particle detachment from crystalline carriers in adhesive mixtures for inhalation. Int. J. Pharm. 327, 17–25.
Edwards, D.A., Hanes, J., Caponetti, G., Hrkach, J., Ben-Jebria, A., Eskew, M.L., Mintzes, J., Deaver, D., Lotan, N., Langer, R., 1997. Large porous particles for pulmonary drug delivery. Science 276, 1868.
Elajnaf, A., Carter, P., Rowley, G., 2006. Electrostatic characterisation of inhaled powders: effect of contact surface and relative humidity. Eur. J. Pharm. Sci. 29, 375–384.
Feeley, J.C., York, P., Sumby, B.S., Dicks, H., 1998. Determination of surface properties and flow characteristics of salbutamol sulphate, before and after micronisation. Int. J. Pharm. 172, 89–96.
Ferron, G.A., 1994. Aerosol properties and lung deposition. Eur. Respir. J. 7, 1392.
Frijlink, H.W., De Boer, A.H., 2004. Dry powder inhalers for pulmonary drug delivery. Edd. 1, 67–86.
Fukuoka, E., Kimura, S., 1992. Cohesion of particulates solids. VIII. Influence of particle shape on compression by tapping. Chem. Pharm. Bull. 40, 2805–2809.
Ganderton, D., Kassem, N.M., 1992. Dry powder inhalers. Adv. Pharm. Sci. 6, 165–191.
Hamishehkar, H., Emami, J., Najafabadi, A.R., Gilani, K., Minaiyan, M., Mahdavi, H., Nokhodchi, A., 2010. Effect of carrier morphology and surface characteristics on the development of respirable PLGA microcapsules for sustained-release pulmonary delivery of insulin. Int. J. Pharm. 389, 74–85.
Haque, M., Roos, Y., 2005. Crystallization and X-ray diffraction of spray-dried and freeze-dried amorphous lactose. Carbohydr. Res. 340, 293–301.
Hassan, M.S., Lau, R.W.M., 2009. Effect of particle shape on dry particle inhalation: study of flowability, aerosolization, and deposition properties. AAPS Pharm. Sci. Technol. 10, 1252–1262.
Hausner, H.H., 1967. Friction conditions in a mass of metal powder. Powder Metall. 13, 7–13.
Hawe, A., Frie, W., 2006. Impact of freezing procedure and annealing on the physico-chemical properties and the formation of mannitol hydrate in mannitol–sucrose–NaCl formulations. Eur. J. Pharm. Biopharm. 64, 316–325.
Hersey, J.A., 1975. Ordered mixing: a new concept in powder mixing practice. Powder Technol. 11, 41–44.
Heyder, J., Gebhart, J., Rudolf, G., Schiller, C.F., Stahlhofen, W., 1986. Deposition of particles in the human respiratory tract in the size range 0.005–15 μm. J. Aerosol Sci. 17, 811–825.
Hickey, A.J., Fults, K.A., Pillai, R.S., 1992. Use of particle morphology to influence the delivery of drug from dry powder aerosols. J. Biopharm. Sci. 3, 2.
Hino, T., Serigano, T., Yamamoto, H., Takeuchi, H., Niwa, T., Kawashima, Y., 1998. Particle design of wogon extract dry powder for inhalation aerosols with granulation method. Int. J. Pharm. 168, 59–68.
Iida, K., Hayakawa, Y., Okamoto, H., Danjo, K., Leuenberger, H., 2003. Preparation of dry powder inhalation by surface treatment of lactose carrier particles. Chem. Pharm. Bull. 51, 1–5.
Iida, K., Hayakawa, Y., Okamoto, H., Danjo, K., Leuenberger, H., 2001. Evaluation of flow properties of dry powder inhalation of salbutamol sulfate with lactose carrier. Chem. Pharm. Bull. 49, 1326–1330.
Iida, K., Leuenberger, H., Fueg, L.M., Muller-Walz, R., Okamoto, H., Danjo, K., 2000. Effect of mixing of fine carrier particles on dry powder inhalation property of salbutamol sulfate (SS). Yakugaku Zasshi J. Pharm. Soc. Jpn. 120, 113–119.
Islam, N., Stewart, P., Larson, I., Hartley, P., 2004. Lactose surface modification by decantation: are drug-fine lactose ratios the key to better dispersion of salmeterol xinafoate from lactose-interactive mixtures? Pharm. Res. 21, 492–499.
Jiang, R.G., Pan, W.S., Wang, C.L., Liu, H., 2005. Use of recrystallized lactose as carrier for inhalation powder of interferon α 2b. Pharmazie 60, 632–633.
Jones, F.T., Lee, K.S., 1970. The optical and crystallographic properties of three phases of mannitol. Microscope 18, 279–285.
Kaialy, W., Ticehurst, M.D., Murphy, J., Nokhodchi, A., 2011b. Improved aerosolization performance of salbutamol sulfate formulated with lactose crystallized from binary mixtures of ethanol–acetone. J. Pharm. Sci. 100, 2665–2684.
Kaialy, W., Momin, M.N., Ticehurst, M.D., Murphy, J., Nokhodchi, A., 2010b. Engineered mannitol as an alternative carrier to enhance deep lung penetration of salbutamol sulphate from dry powder inhaler. Colloids Surface B-Biointerfaces 79, 345–356.
Kaialy, W., Martin, G.P., Ticehurst, M.D., Momin, M.N., Nokhodchi, A., 2010a. The enhanced aerosol performance of salbutamol from dry powders containing engineered mannitol as excipient. Int. J. Pharm. 392, 178–188.
Kaialy, W., Martin, G.P., Ticehurst, M.D., Larhrib, H., Kolosionek, E., Nokhodchi, A. The influence of physical properties and morphology of crystallised lactose on delivery of salbutamol sulphate from dry powder inhalers, Colloids Surface B-Biointerfaces, doi:10.1016/j.colsurfb.2011.08.019, in press.
Kaialy, W., Martin, G.P., Ticehurst, M.D., Royall, P., Mohammad, M.A., Murphy, J., Nokhodchi, A., 2011a. Characterisation and deposition studies of recrystallised lactose from binary mixtures of ethanol/butanol for improved drug delivery from dry powder inhalers. AAPS J. 13, 30–43.
Kawashima, Y., Serigano, T., Hino, T., Yamamoto, H., Takeuchi, H., 1998. Effect of surface morphology of carrier lactose on dry powder inhalation property of pranlukast hydrate. Int. J. Pharm. 172, 179–188.
Kumar, P., Santosa, J.K., Beck, E., Das, S., 2004. Direct-write deposition of fine powders through miniature hopper-nozzles for multi-material solid freeform fabrication. Rapid Prototyping J. 10, 14–23.
Kumar, V., Kothari, S.H., Banker, G.S., 2001. Compression, compaction, and disintegration properties of low crystallinity celluloses produced using different agitation rates during their regeneration from phosphoric acid solutions. AAPS Pharm. Sci. Technol. 2, 22–28.
Larhrib, H., Zeng, X.M., Martin, G.P., Marriott, C., Pritchard, J., 1999. The use of different grades of lactose as a carrier for aerosolised salbutamol sulphate. Int. J. Pharm. 191, 1–14.
Lippmann, M., Timbrell, V., 1990. Particle loading in the human lung–human experience and implications for exposure limits. J. Aerosol Med. 3, 155–168.
Louey, M.D., Stewart, P.J., 2002. Particle interactions involved in aerosol dispersion of ternary interactive mixtures. Pharm. Res. 19, 1524–1531.
Louey, M.D., Razia, S., Stewart, P.J., 2003. Influence of physico-chemical carrier properties on the in vitro aerosol deposition from interactive mixtures. Int. J. Pharm. 252, 87–98.
Malcolmson, R.J., Embleton, J.K., 1998. Dry powder formulations for pulmonary delivery. Pharm. Sci. Technol. Today 1, 394–398.
Martonen, T.B., Katz, I., Fults, K., Hickey, A.J., 1992. Use of analytically defined estimates of aerosol respirable fraction to predict lung deposition patterns. Pharm. Res. 9, 1634–1639.
Mitchell, J.P., Nagel, M.W., 2003. Cascade impactors for the size characterization of aerosols from medical inhalers: their uses and limitations. J. Aerosol Med. 16, 341–377.
Murakoshi, H., Saotome, T., Fujii, Y., Ozeki, T., Takashima, Y., Yuasa, H., Okada, H., 2005. Effect of physical properties of carrier particles on drug emission from a dry powder inhaler device. J. Drug Deliv. Sci. Technol. 15, 223–226.
Nakate, T., Yoshida, H., Ohike, A., Tokunaga, Y., Ibuki, R., Kawashima, Y., 2004. Formulation development of inhalation powders for FK888 with carrier lactose using spinhaler® and its absorption in healthy volunteers. J. Control. Release 97, 19–29.
Neumann, A.M., Kramer, H.J.M., 2002. A comparative study of various size distribution. Part. Part. Syst. Character. 19, 17–27.
Neumann, B.S., 1967. The flow properties of powders. Adv. Pharm. Sci. 2, 191–221.
Otsuka, A., Iida, K., Danjo, K., Sunada, H., 1988. Measurement of the adhesive force between particles of powdered materials and a glass substrate by means of the impact separation method. III. Effect of particle shape and surface asperity. Chem. Pharm. Bull. 36, 741–749.
Price, A.H., Clissold, S.P., 1989. Salbutamol in the 1980. A reappraisal of its clinical efficacy. Drugs 38, 77–122.
Prime, D., Atkins, P.J., Slater, A., Sumby, B., 1997. Review of dry powder inhalers. Adv. Drug Deliv. Rev. 26, 51–58.
Rabbani, N.R., Seville, P.C., 2005. The influence of formulation components on the aerosolisation properties of spray-dried powders. J. Control. Release 110, 130–140.
Raghavan, S.L., Ristic, R.I., Sheen, D.B., Sherwood, J.N., Trowbridge, L., York, P., 2000. Articles-physical chemistry of surfaces and interfaces-morphology of crystals of a-lactose hydrate grown from aqueous solution. J. Phys. Chem. B 104, 12256–12262.
Rajniak, P., Mancinelli, C., Chern, R.T., Stepanek, F., Farber, L., Hill, B.T., 2007. Experimental study of wet granulation in fluidized bed: impact of the binder properties on the granule morphology. Int. J. Pharm. 334, 92–102.
Raula, J., Kurkela, J.A., Brown, D.P., Kauppinen, E.I., 2007. Study of the dispersion behaviour of L-leucine containing microparticles synthesized with an aerosol flow reactor method. Powder Technol. 177, 125–132.
Rowe, R.C., Sheskey, P.J., Weller, P.J., 2003. Handbook of Excipients, 6th ed. Pharmaceutical Press, London, 365.
Sethuraman, V.V., Hickey, A.J., 2002. Powder properties and their influence on dry powder inhaler delivery of an antitubercular drug. AAPS Pharm. Sci. Technol. 3, 7–16.
Seville, P.C., Kellaway, I.W., Birchall, J.C., 2002. Preparation of dry powder gene delivery systems for pulmonary administration. Proc. Drug Deliv. Lungs, 172–175.
Sharma, V.K., Kalonia, D.S., 2004. Effect of vacuum drying on protein-mannitol interactions: the physical state of mannitol and protein structure in the dried state. AAPS Pharm. Sci. Technol. 5, 58–69.
Smyth, H.D.C., Hickey, A.J., 2005. Carriers in drug powder delivery: implications for inhalation system design. Am. J. Drug Del. 3, 117–132.
Stahlhofen, W., Gebhart, J., Heyder, J., 1980. Experimental determination of the regional deposition of aerosol particles in the human respiratory tract. Am. Ind. Hyg. Assoc. J. 41, 385–398.
Staniforth, J.N., Rees, J.E., Lai, F.K., Hersey, J.A., 1982. Interparticle forces in binary and ternary ordered powder mixes. J. Pharm. Pharmacol. 34, 141–145.
Steckel, H., Müller, B.W., 1997. In vitro evaluation of dry powder inhalers. II. Influence of carrier particle size and concentration on in vitro deposition. Int. J. Pharm. 154, 31–37.
Steckel, H., Borowski, M., Eskandar, F., Villax, P., 2004. Solid dosage selecting lactose for a capsule-based dry powder inhaler. Pharm. Technol. Eur. 16, 23–36.
Tang, P., Chan, H.K., Chiou, H., Ogawa, K., Jones, M.D., Adi, H., Buckton, G., Prud'homme, R.K., Raper, J.A., 2009. Characterisation and aerosolisation of mannitol particles produced via confined liquid impinging jets. Int. J. Pharm. 367, 51–57.
Telko, M.J., Hickey, A.J., 2005. Dry powder inhaler formulation. Respir. Care 50, 1209–1227.
Timsina, M.P., Martin, G.P., Marriott, C., Ganderton, D., Yianneskis, M., 1994. Drug delivery to the respiratory tract using dry powder inhalers. Int. J. Pharm. 101, 1–13.

Tinke, A.P., Carnicer, A., Govoreanu, R., Scheltjens, G., Lauwerysen, L., Mertens, N., Vanhoutte, K., Brewster, M.E., 2008. Particle shape and orientation in laser diffraction and static image analysis size distribution analysis of micrometer sized rectangular particles. Powder Technol. 186, 154–167.

Traini, D., Young, P.M., Thielmann, F., Acharya, M., 2008. The influence of lactose pseudopolymorphic form on salbutamol sulfate-lactose interactions in DPI formulations. Drug Dev. Ind. Pharm. 34, 992–1001.

USP Pharmacopeia, 2003. The Official Compendia of Standards, USP 26/NF 21. United States Pharmacopeial Conventio, Inc., Rockville, MD, Aerosols <601>, 2114–2123.

Van Kreveld, A., Michaels, A.S., 1965. Measurement of crystal growth rates in lactose crystals. J. Dairy Sci. 48, 259–265.

Vanbever, R., Mintzes, J.D., Wang, J., Nice, J., Chen, D., Batycky, R., Langer, R., Edwards, D.A., 1999. Formulation and physical characterization of large porous particles for inhalation. Pharm. Res. 16, 1735–1742.

Velaga, S.P., Bergh, S., Carlfors, J., 2004. Stability and aerodynamic behaviour of glucocorticoid particles prepared by a supercritical fluids process. Eur. J. Pharm. Sci. 21, 501–509.

Walter-Levy, L., 1968. Cristallochimie-sur les variétés cristallines du D-mannitol. CR Acad. Sci. Paris Ser. C 267, 1779–1782.

Yoshinari, T., Forbes, R.T., York, P., Kawashima, Y., 2002. Moisture induced polymorphic transition of mannitol and its morphological transformation. Int. J. Pharm. 247, 69–77.

Young, P.M., Price, R., 2004. The influence of humidity on the aerosolisation of micronised and SEDS produced salbutamol sulphate. Eur. J. Pharm. Sci. 22, 235–240.

Young, P.M., Edge, S., Traini, D., Jones, M.D., Price, R., El-Sabawi, D., Urry, C., Smith, C., 2005. The influence of dose on the performance of dry powder inhalation systems. Int. J. Pharm. 296, 26–33.

Yu, L., Milton, N., Groleau, E.G., Mishra, D.S., Vansickle, R.E., 1999. Existence of a mannitol hydrate during freeze-drying and practical implications. J. Pharm. Sci. 88, 196–198.

Zeng, X.M., Martin, G.P., Marriott, C., 2001a. Particulate Interactions in Dry Powder Formulations for Inhalation, 1st ed. Informa HealthCare, 30–249.

Zeng, X.M., Martin, G.P., Marriott, C., Pritchard, J., 2001b. Lactose as a carrier in dry powder formulations: the influence of surface characteristics on drug delivery. J. Pharm. Sci. 90, 1424–1434.

Zeng, X.M., Martin, G.P., Marriott, C., Pritchard, J., 2000. The influence of carrier morphology on drug delivery by dry powder inhalers. Int. J. Pharm. 200, 93–106.